CHAPTER

Energy Release Rate

4

Linear elastic fracture mechanics (LEFM) can be studied by either the near-tip stress field or the energy method. In the near-tip stress field approach discussed in Chapter 3, crack growth is determined by the local stress field around the crack tip, which is characterized by the stress intensity factor. Fracture occurs when the stress intensity factor reaches its critical value, that is, the fracture toughness. It was Irwin [4-1] who introduced the concept of stress intensity factor that drew focus on the near-tip stress and displacement fields theory.

In the energy approach introduced in this chapter, the fracture behavior of a material is described by the energy variation of the cracked system during crack extension, which is characterized by the so-called energy release rate. The energy release is considered a global exercise of the cracked system. Griffith's original concept of fracture was based on the energy released during crack extension. This method was later further developed by Irwin [4-2] and Orowan [4-3]. For linear elastic materials, the energy and the stress field approaches can be considered equivalent.

4.1 THE CONCEPT OF ENERGY RELEASE RATE

Consider a two dimensional elastic body occupying an area A_0 with the boundary Γ. It is assumed that Γ consists of Γ_t and Γ_u, with Γ_t and Γ_u being the portions of the boundary with prescribed tractions and prescribed displacements, respectively. The total potential energy per unit thickness is defined as

$$\Pi = U + V \tag{4.1}$$

where

$$U = \iint_{A_0} W dA \tag{4.2}$$

Fracture Mechanics. DOI: 10.1016/B978-0-12-385001-0.00004-3

is the total strain energy stored in the elastic body, and

$$V = -\int_{\Gamma_t} T_i u_i d\Gamma \tag{4.3}$$

is the potential of external forces. In Eqs. (4.2) and (4.3), T_i are the prescribed tractions on Γ_t, u_i are the corresponding displacements, and W is the strain energy density given by

$$W = W(e_{ij}) = \int_0^{e_{ij}} \sigma_{ij} de_{ij} \tag{4.4}$$

where σ_{ij} is the stress tensor and e_{ij} is the strain tensor. For linear elastic materials, W can be expressed as follows:

$$W = \frac{1}{2}\sigma_{ij} e_{ij}$$

The energy method of LEFM involves total potential energy variation of a cracked system during crack growth. The energy release rate G is defined as total potential energy decrease during unit crack extension, that is,

$$G = -\frac{d\Pi}{da} \tag{4.5}$$

where a is the crack length and da is the crack extension. If the elastic body is free from external tractions, the potential energy becomes the strain energy, that is, $\Pi = U$. The energy release rate is then equivalent to the strain energy release rate. Corresponding to the criterion Eq. (3.117) in Chapter 3, the fracture criterion in the energy approach is

$$G = G_c \tag{4.6}$$

where G_c is the critical value of G. In the Griffith theory discussed in Chapter 2, G_c is two times surface energy γ_c, which applies to perfectly brittle solids. Irwin [4-2] and Orowan [4-3] extended the preceding criterion to metals experiencing small-scale yielding by lumping the surface energy and the plastic energy dissipation into G_c.

4.2 THE RELATIONS BETWEEN *G* AND *K* BY THE CRACK CLOSURE METHOD

The energy and the near-tip stress field approaches for the fracture of elastic bodies are equivalent, that is, there exists a unique relation between the energy release rate and the stress intensity factor. This relationship can be established by the so-called crack closure method.

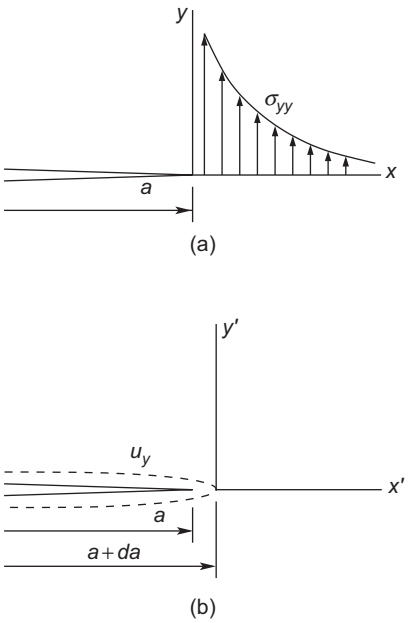

FIGURE 4.1

Virtual crack extension and crack closure method: (a) before extension of *da*, (b) after extension of *da*.

First consider a Mode I crack before and after an extension of *da* as shown in Figures 4.1(a) and (b), respectively. From (3.44) in Section 3.7, the normal stress σ_{yy} ahead of the crack tip ($\theta = 0$) (before extension) is

$$\sigma_{yy} = \frac{K_I(a)}{\sqrt{2\pi x}} \tag{4.7}$$

where $K_I(a)$ is the stress intensity factor and the origin of the coordinate system $x - y$ is at the crack tip.

After the assumed crack extension of *da*, new crack surfaces are created in $0 \leq x \leq da$ and the displacement of its upper face is given by (3.45), which can be written in terms of the $x' - y'$ coordinates (with the origin at the grown crack tip) as

$$u_y = \frac{\kappa + 1}{4\mu\pi} K_I \sqrt{2\pi(-x')}$$

Noting that $x' = x - da$, we rewrite this expression as

$$u_y = \frac{\kappa + 1}{4\mu\pi} K_I \sqrt{2\pi(da - x)} \tag{4.8}$$

where $K_I = K_I(a + da)$. Because da is vanishingly small, K_I in Eq. (4.8) can be taken to be equal to $K_I(a)$.

The strain energy released associated with the crack extension da can be regarded as the work done by the stress σ_{yy} in Eq. (4.7) before crack extension, which closes up the crack opening Eq. (4.8) in the region $-da \le x' \le 0$ after crack extension, that is, the work done by σ_{yy} in Eq. (4.7) traversing u_y in Eq. (4.8) is equal to the energy released $G_I\, da$, where G_I is the energy release rate for Mode I. We thus have

$$G_I\, da = 2\int_0^{da} \frac{1}{2}\sigma_{yy} u_y\, dx$$

where the factor 2 on the right side accounts for the two (upper and lower) crack surfaces. Substitution of Eqs. (4.7) and (4.8) into the previous expression yields

$$G_I\, da = \frac{\kappa + 1}{4\mu\pi} K_I^2 \int_0^{da} \sqrt{\frac{1 - x/da}{x/da}}\, dx \tag{4.9}$$

With the new integral variable η defined by

$$x = da \sin^2 \eta$$
$$dx = da \cdot 2 \sin\eta \cos\eta\, d\eta$$

the integral in Eq. (4.9) can be evaluated as

$$\begin{aligned}\int_0^{da} \sqrt{\frac{1 - x/da}{x/da}}\, dx &= 2\, da \int_0^{\pi/2} \sqrt{\frac{\cos^2\eta}{\sin^2\eta}}\, \sin\eta\cos\eta\, d\eta \\ &= 2da \int_0^{\pi/2} \cos^2\eta\, d\eta \\ &= \frac{\pi}{2}\, da\end{aligned}$$

With this integral, we have

$$G_I\, da = \frac{\kappa + 1}{8\mu} K_I^2\, da$$

Thus,

$$G_I = \frac{\kappa + 1}{8\mu} K_I^2 \tag{4.10}$$

For plane strain, $\kappa = 3 - 4\nu$, and we have

$$G_I = \frac{(1-\nu)}{2\mu} K_I^2 = \frac{(1-\nu^2)}{E} K_I^2 \tag{4.11}$$

For plane stress, $\kappa = (3-\nu)/(1+\nu)$, and

$$G_I = \frac{K_I^2}{2\mu(1+\nu)} = \frac{K_I^2}{E} \tag{4.12}$$

For Mode II and Mode III problems, if the crack is assumed to grow in its original direction (a Mode II crack generally deflects from the original crack direction; see discussons in Chapter 5), we can obtain similar relations between G and K as

$$G_{II} = \frac{\kappa+1}{8\mu} K_{II}^2 \tag{4.13}$$

$$G_{III} = \frac{1}{2\mu} K_{III}^2 \tag{4.14}$$

respectively.

An alternative approach for deriving the strain energy release rates is to calculate the total strain energy released during the process of crack formation from $a = 0$ to a. Consider a Mode III crack of length $2a$ in an infinite body subjected to remote shearing stress. The total strain energy may be decomposed into two parts, that is, $U_{III} = U_{IIInc} + U_{IIIc}$, where U_{IIIc} is due to the presence of the crack and U_{IIInc} is independent of crack length. According to the crack closure approach, the strain energy due to the crack is

$$U_{IIIc} = 4 \int_0^a \frac{1}{2} S u_z \, dx \tag{4.15}$$

where S is the corresponding remote anti-plane shear stress. Substituting the upper crack surface displacement Eq. (3.70),

$$u_z = \frac{S}{\mu} \sqrt{a^2 - x^2}$$

in Eq. (4.15), we obtain

$$\begin{aligned} U_{IIIc} &= 2 \int_0^a \frac{S^2}{\mu} \sqrt{a^2 - x^2} \, dx \\ &= 2 \frac{S^2}{\mu} \left[\frac{1}{2} x \sqrt{a^2 - x^2} + \frac{1}{2} a^2 \sin^{-1} \left(\frac{x}{a} \right) \right]_0^a \\ &= \frac{\pi S^2 a^2}{2\mu} \end{aligned} \tag{4.16}$$

The energy release rate per crack tip is

$$G_{III} = \frac{dU_{III}}{d(2a)} = \frac{1}{2}\frac{dU_{IIIc}}{da} = \frac{K_{III}^2}{2\mu} \tag{4.17}$$

The relations between the strain energy release rates and the stress intensity factors allow one to calculate either parameter using the most efficient method available.

4.3 THE *J*-INTEGRAL

In fracture mechanics, Rice [4-4], [4-5] first derived the contour *J*-integral from the potential energy variation with crack extension. The *J*-integral theory holds for both linear and nonlinear elastic materials. The concept has been used for elastic-plastic materials obeying deformation plasticity, which will be discussed in Chapter 6.

The *J*-integral defined by Rice [4-4] has the following expression:

$$J = \int_{\Gamma} \left(W dy - T_i \frac{\partial u_i}{\partial x} d\Gamma \right) = \int_{\Gamma} \left(W n_1 - \sigma_{ij} \frac{\partial u_i}{\partial x} n_j \right) d\Gamma \tag{4.18}$$

where the summation convention over the dummy index i is observed and i takes 1 and 2, or x and y, Γ is an arbitrary contour beginging at the lower crack surface and ending on the upper crack surface, as shown in Figure 4.2 (Γ_1, for example), n_j are the components of the unit outward vector normal to the contour, and $T_i = \sigma_{ij} n_j$ are the tractions along the contour. It will be seen that the *J*-integral is the energy release rate for crack growth in an elastic body. The *J*-integral also represents a kind

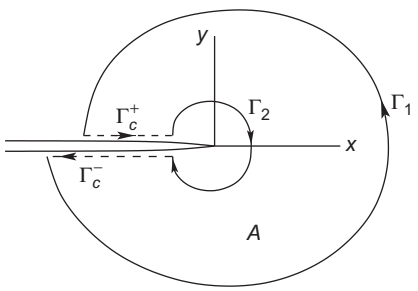

FIGURE 4.2

Integration contours in a cracked body.

of conservation property because of its path-independence. These properties of the J-integral can be proved using the following basic equations of elasticity:

$$\sigma_{ij,j} = 0 \quad \text{(equilibrium equation)} \tag{4.19}$$

$$e_{ij} = \frac{1}{2}\left(u_{i,j} + u_{j,i}\right) \quad \text{(strain-displacement relation)} \tag{4.20}$$

$$\sigma_{ij} = \frac{\partial W}{\partial e_{ij}} \quad \text{(stress–strain relation)} \tag{4.21}$$

4.3.1 *J* as Energy Release Rate

Consider a two-dimensonal cracked body with an area A_0 enclosed by the boundary Γ_0, as shown in Figure 4.3. The boundary Γ_0 consists of the outer contour Γ and the crack surfaces Γ_a. The elastic medium is subjected to the prescribed traction T_i along the boundary segment Γ_t and the prescribed displacements on the boundary segment Γ_u. The crack surfaces are along the X-axis and are assumed to be free of traction. The positive contour direction of Γ_0 is defined in that when one travels along it, the domain of interest always lies to the left of the traveler. It follows from Eqs. (4.1) to (4.3) that the potential energy Π of the cracked system per unit thickness can be written as

$$\Pi = \Pi(a) = \iint_{A_0} W dX dY - \int_{\Gamma_t} T_i u_i d\Gamma$$

where a is the crack length and (X, Y) is a stationary Cartesian coordinate system. The body forces are absent.

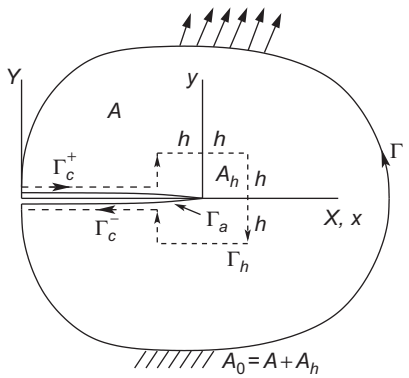

FIGURE 4.3

Contours and coordinate systems in a cracked body.

Now evaluate the energy release rate defined by

$$G = -\frac{d\Pi}{da} = -\frac{d}{da}\iint_{A_0} W dX dY + \frac{d}{da}\int_{\Gamma_t} T_i u_i d\Gamma \tag{4.22}$$

It is known from Chapter 3 that W has a $1/r$ singularity at the crack tip (r is the distance from the tip) in LEFM. Thus, the differentiation with respect to the crack length may not be directly performed within the area integral sign in Eq. (4.22) because the differentiation with respect to a will involve the derivation with respect to r as seen in the following.

We now consider a small square A_h with the center at the crack tip as shown in Figure 4.3. The side length of the square is $2h$ and the boundary is denoted by Γ_h. The region of the cracked body excluding A_h is denoted by A, that is,

$$A_0 = A \cup A_h$$

Because no stress singularity exists in A and along Γ_t, Eq. (4.22) can be written as

$$\begin{aligned} G &= -\frac{d}{da}\left[\iint_A W dX dY + \iint_{A_h} W dX dY\right] + \int_{\Gamma_t} T_i \frac{du_i}{da} d\Gamma \\ &= -\iint_A \frac{dW}{da} dX dY + \int_{\Gamma_0} T_i \frac{du_i}{da} d\Gamma - \frac{d}{da}\iint_{A_h} W dX dY \end{aligned} \tag{4.23}$$

Here, the integration along Γ_t is extended to the entire boundary Γ_0 because $T_i = 0$ on the crack faces Γ_a and $du_i/da = 0$ on Γ_u. It is convenient to introduce a local coordinate system (x, y) attached at the crack tip, that is,

$$x = X - a, \quad y = Y$$

Thus,

$$\frac{d(\,)}{da} = \frac{\partial(\,)}{\partial a} - \frac{\partial(\,)}{\partial x} \tag{4.24}$$

when the field variables are described in the local coordinate system (x, y). Using relationship Eq. (4.24), Eq. (4.23) can be written as

$$\begin{aligned} G = &-\iint_A \frac{\partial W}{\partial a} dx dy + \int_{\Gamma_0} T_i \frac{\partial u_i}{\partial a} d\Gamma \\ &+ \iint_A \frac{\partial W}{\partial x} dx dy - \int_{\Gamma_0} T_i \frac{\partial u_i}{\partial x} d\Gamma - \frac{d}{da}\iint_{A_h} W dX dY \end{aligned} \tag{4.25}$$

Note that on the crack surface $T_i = dy = 0$. Use of the divergence theorem thus gives

$$\iint_A \frac{\partial W}{\partial x} dA = \int_{\Gamma+\Gamma_h} W n_x d\Gamma = \int_{\Gamma+\Gamma_h} W dy \tag{4.26}$$

and

$$\begin{aligned}\iint_A \frac{\partial W}{\partial a} dxdy &= \iint_A \frac{\partial}{\partial x_j}\left(\sigma_{ij}\frac{\partial u_i}{\partial a}\right) dxdy \\ &= \int_{\Gamma+\Gamma_h} \sigma_{ij} n_j \frac{\partial u_i}{\partial a}\, d\Gamma \\ &= \int_{\Gamma+\Gamma_h} T_i \frac{\partial u_i}{\partial a}\, d\Gamma \\ &= \int_{\Gamma_0+\Gamma_h} T_i \frac{\partial u_i}{\partial a}\, d\Gamma \end{aligned} \tag{4.27}$$

In deriving Eq. (4.27), the following relation has been used:

$$\begin{aligned}\frac{\partial W}{\partial a} &= \frac{\partial W}{\partial e_{ij}}\frac{\partial e_{ij}}{\partial a} = \sigma_{ij}\frac{\partial}{\partial a}\left(\frac{\partial u_i}{\partial x_j}\right) \\ &= \sigma_{ij}\frac{\partial}{\partial x_j}\left(\frac{\partial u_i}{\partial a}\right) \\ &= \frac{\partial}{\partial x_j}\left(\sigma_{ij}\frac{\partial u_i}{\partial a}\right) - \frac{\partial u_i}{\partial a}\frac{\partial \sigma_{ij}}{\partial x_j} \\ &= \frac{\partial}{\partial x_j}\left(\sigma_{ij}\frac{\partial u_i}{\partial a}\right) \end{aligned} \tag{4.28}$$

where all elasticity Eqs. (4.19), (4.20), and (4.21) have been used. Using Eqs. (4.26) and (4.27), Eq. (4.25) becomes

$$\begin{aligned} G = &\int_\Gamma W dy - \int_\Gamma T_i \frac{\partial u_i}{\partial x} d\Gamma \\ &+ \int_{\Gamma_h} W dy - \int_{\Gamma_h} T_i \frac{\partial u_i}{\partial a} d\Gamma - \frac{d}{da}\iint_{A_h} W dX dY \end{aligned} \tag{4.29}$$

Here again the condition that $T_i = 0$ on the crack faces Γ_a is used so that the second integral on the right side of Eq. (4.29) is reduced to the outer contour Γ.

The strain energy density function has the following universal separable form in the region near the moving crack tip:

$$W = B(a)\widetilde{W}(X-a,Y) = B(a)\widetilde{W}(x,y) \tag{4.30}$$

where $B(a)$ may depend on loading and other factors but not on the local coordinates, and $\widetilde{W}(x,y)$ is a function of local coordinates only. Now assume that A_h is so small that Eq. (4.30) holds in a region containing A_h. It has been shown in [4-6] that

$$\begin{aligned}\frac{d}{da}\iint_{A_h} W dX dY &= \int_{\Gamma_h} W dy + \iint_{A_h} \frac{\partial W}{\partial a} dx dy \\ &= \int_{\Gamma_h} W dy - \int_{\Gamma_h} T_i \frac{\partial u_i}{\partial a} d\Gamma\end{aligned}$$

Substituting this relation into Eq. (4.29) leads to

$$G = \int_{\Gamma} \left(W dy - T_i \frac{\partial u_i}{\partial x} d\Gamma \right)$$

The integral on the right side of this is the J-integral in Eq. (4.18). Hence, the J-integral is the energy release rate.

4.3.2 Path-Independence

In deriving the J-integral in Section 4.3.1 the integral is taken along the boundary of the edge-cracked body, excluding the crack surfaces. In fact, the integration contour Γ can be arbitrarily selected as long as it begins at the lower crack face and ends on the upper crack face, which is the original definition of Rice [4-4]. This is the path-independence of the J-integral. To prove this conservation property, choose a closed-contour Γ_T that consists of contours Γ_1, Γ_2, and Γ_c^+, Γ_c^- as shown in Figure 4.2. Clearly, there is no stress singularity in the area A enclosed by Γ_T.

Consider the contour integral along Γ_T:

$$\int_{\Gamma_T} \left(W n_x - \sigma_{ij} n_j \frac{\partial u_i}{\partial x} \right) d\Gamma$$

Applying the divergence theorem, we have

$$\int_{\Gamma_T} \left(W n_x - \sigma_{ij} n_j \frac{\partial u_i}{\partial x} \right) d\Gamma = \int_A \left[\frac{\partial W}{\partial x} - \frac{\partial}{\partial x_j} \left(\sigma_{ij} \frac{\partial u_i}{\partial x} \right) \right] dA \tag{4.31}$$

Note from Eq. (4.28) that

$$\frac{\partial W}{\partial x} = \frac{\partial}{\partial x_j}\left(\sigma_{ij}\frac{\partial u_i}{\partial x}\right)$$

Substituting this expression into Eq. (4.31) leads to the conclusion that

$$\int_{\Gamma_T}\left(Wn_x - \sigma_{ij}n_j\frac{\partial u_i}{\partial x}\right)d\Gamma = 0 \tag{4.32}$$

Noting that the crack surfaces are traction free, Eq. (4.32) becomes

$$\circlearrowleft\int_{\Gamma_1}\left(Wdy - T_i\frac{\partial u_i}{\partial x_x}\,d\Gamma\right) + \circlearrowright\int_{\Gamma_2}\left(Wdy - T_i\frac{\partial u_i}{\partial x}\,d\Gamma\right) = 0$$

Reversing the direction of contour Γ_2, we obtain

$$\circlearrowleft\int_{\Gamma_1}\left(Wdy - T_i\frac{\partial u_i}{\partial x}\,d\Gamma\right) = \circlearrowleft\int_{\Gamma_2}\left(Wdy - T_i\frac{\partial u_i}{\partial x}\,d\Gamma\right)$$

This implies that the J-integral

$$J = \int_{\Gamma_1}\left(Wdy - T_i\frac{\partial u_i}{\partial x}\,d\Gamma\right)$$

is path-independent.

4.3.3 Relation between *J* and *K*

Because J is the energy release rate G, the relation between G and the stress intensity factor K also holds for J and K, that is,

$$J = \frac{\kappa+1}{8\mu}\left(K_I^2 + K_{II}^2\right) + \frac{1}{2\mu}K_{III}^2 \tag{4.33}$$

under the general mixed mode fracture cases. The preceding relationship may also be derived using Eq. (4.18) and the crack tip stress and displacement fields introduced in Chapter 3. Here the Cherepanov contour [4-7] near the crack tip is used. Since the J-integral is path-independent, we can select any path that offers the most simplicity for the integration.

Consider an integration path along the boundary of a narrow rectangle with the center at the crack tip, as shown in Figure 4.4. The length and the width of the rectangle are 2ε and 2δ, respectively. It is assumed that the rectangle is vanishingly thin

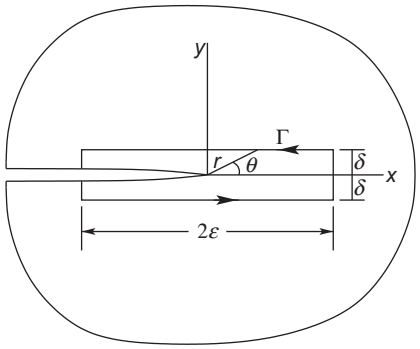

FIGURE 4.4

Cherepanov contour around a crack tip for evaluation of the J-integral.

and is within the K-dominance zone, that is, $\delta << \varepsilon$ and $\varepsilon \to 0$. Thus, the integral over the vertical lines of the contour can be neglected, and the J-integral reduces to the integral along the upper and lower horizontal lines

$$J = \lim_{\varepsilon \to 0} \int_{-\varepsilon}^{\varepsilon} \left(\sigma_{xy} \frac{\partial u_x}{\partial x} + \sigma_{yy} \frac{\partial u_y}{\partial x} + \sigma_{zy} \frac{\partial u_z}{\partial x} \right) \Bigg|_{y=-\delta \to 0^-} dx$$

$$+ \lim_{\varepsilon \to 0} \int_{\varepsilon}^{-\varepsilon} \left(\sigma_{xy} \frac{\partial u_x}{\partial x} + \sigma_{yy} \frac{\partial u_y}{\partial x} + \sigma_{zy} \frac{\partial u_z}{\partial x} \right) \Bigg|_{y=\delta \to 0^+} dx \tag{4.34}$$

Note that in this integral $d\Gamma = -dx$ has been used for the upper contour. First consider the case of Mode I. Due to symmetry consideration ($\sigma_{yy}\big|_{y=0^-} = \sigma_{yy}\big|_{y=0^+}$, $u_y\big|_{y=0^-} = -u_y\big|_{y=0^+}$), Eq. (4.34) reduces to

$$J = 2 \lim_{\varepsilon \to 0} \int_{\varepsilon}^{-\varepsilon} \sigma_{yy} \frac{\partial u_y}{\partial x} \Bigg|_{y=\delta \to 0^+} dx \tag{4.35}$$

where the factor 2 accounts for the two horizontal lines.

The near-tip stress and displacement fields are

$$\sigma_{yy} = \frac{K_I}{\sqrt{2\pi r}} \cos\frac{\theta}{2} \left[1 + \sin\frac{\theta}{2} \sin\frac{3}{2}\theta \right]$$

$$u_y = \frac{K_I}{8\mu\pi} \sqrt{2\pi r} \left[(2\kappa + 1) \sin\frac{\theta}{2} - \sin\frac{3\theta}{2} \right]$$

With some mathematical manipulations, we obtain

$$\frac{\partial u_y}{\partial x} = \frac{\partial u_y}{\partial r}\frac{\partial r}{\partial x} + \frac{\partial u_y}{\partial \theta}\frac{\partial \theta}{\partial x}$$
$$= \frac{K_I}{16\mu\pi}\sqrt{\frac{2\pi}{r}}\left[-(2\kappa+2)\sin\frac{\theta}{2} + 2\sin\theta\cos\frac{3\theta}{2}\right]$$

Along the upper horizontal contour,

$$x = \delta\cot\theta$$

This relation gives

$$dx = -\frac{\delta}{\sin^2\theta}d\theta$$

Thus,

$$\sigma_{yy}\frac{\partial u_y}{\partial x}dx = \frac{K_I^2}{16\mu\pi}[(\kappa+1)\ \frac{\kappa+1}{2}(\cos\theta - \cos 2\theta)$$
$$-(\cos\theta + \cos 2\theta) + \frac{1}{4}(\cos 4\theta - \cos 2\theta)\,]d\theta$$

Substituting the previous expression into Eq. (4.35) yields the J-integral for Mode I cracks:

$$J = 2\int_0^{\pi}\frac{K_I^2}{16\mu\pi}(\kappa+1)\,d\theta = \frac{(\kappa+1)}{8\mu}K_I^2$$

Similarly, Eq. (4.33) can be proved for Mode II and Mode III cracks. This proving procedure also verifies that $J = G$.

4.3.4 Examples

Example 4.1

A semi-infinite crack in an infinite elastic strip. Consider an infinite strip containing a semi-infinite crack as shown in Figure 4.5.

The strip is stretched by a uniform vertical displacement u_0 applied along the upper and lower edges, that is,

$$u_y = \pm u_0, \quad u_x = 0 \qquad \text{at } y = \pm h/2$$

Select the contour Γ for the J-integral as shown in Figure 4.5, that is, Γ consists of Γ_1, Γ_2, Γ_3, Γ_4, and Γ_5, where Γ_1 and Γ_5 are located at $x = -\infty$, Γ_3 is at $x = \infty$, and Γ_2 and Γ_4 are along the lower and upper boundary of the strip, respectively. We readily recognize the

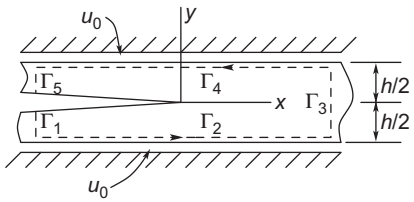

FIGURE 4.5

Integration contour in an infinite strip with a semi-infinite crack for the evaluation of J.

following properties along different segments of the contour:

$$\Gamma_1 \text{ and } \Gamma_5: \quad W = 0, \quad T_i = 0$$

$$\Gamma_2 \text{ and } \Gamma_4: \quad dy = 0, \quad \frac{\partial u_i}{\partial x} = 0$$

$$\Gamma_3: \quad \partial u_i / \partial x = 0$$

Thus, the J-integral reduces to

$$J = \int_{\Gamma_3} W_\infty \, dy = \int_{-h/2}^{h/2} W_\infty \, dy = hW_\infty$$

where W_∞ is the strain energy density at $x = \infty$ and is a constant over the height h.

The uniform deformation field at $x = \infty$ is given by

$$e_{xx} = 0, \qquad e_{yy} = \frac{2u_0}{h}, \qquad e_{xy} = 0$$

From the stress–strain relations Eq. (3.4) for plane elasticity, we have

$$\sigma_{yy} = \frac{\mu(\kappa + 1)}{\kappa - 1} \, e_{yy}$$

Thus,

$$W_\infty = \frac{1}{2} \, \sigma_{yy} e_{yy} = \frac{2\mu(\kappa + 1)u_0^2}{(\kappa - 1)h^2}$$

and

$$J = \frac{2\mu(\kappa + 1)u_0^2}{(\kappa - 1)h}$$

Example 4.2

Double cantilever beam. Consider a double cantilever beam of unit width subjected to a symmetric pair of moments, as shown in Figure 4.6.

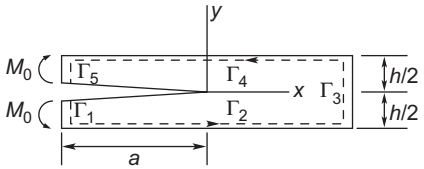

FIGURE 4.6

Integration contour in a double cantilever beam for the evaluation of J.

Assume that a is large as compared with h so that the simple beam theory is adequate for analysis of the split portion of the beam. The unsplit portion is also assumed to be long and, thus, the right end can be considered not loaded. Select the contour for the J-integral, as shown in Figure 4.6. We have

$$\text{along } \Gamma_2 \text{ and } \Gamma_4: \quad dy = 0, \quad T_i = 0$$
$$\text{along } \Gamma_3: \quad W = 0, \quad T_i = u_i = 0$$

Thus, the J-integral reduces to

$$J = \int_{\Gamma_1+\Gamma_5} \left(W dy - T_i \frac{\partial u_i}{\partial x}\, d\Gamma \right)$$
$$= \int_{h/2}^{-h/2} \left(W dy + T_i \frac{\partial u_i}{\partial x}\, dy \right)$$

Note that along Γ_1 and Γ_5 the components of the unit normal vector to the contour are $n_x = -1$ and $n_y = 0$. Thus,

$$J = \int_{h/2}^{-h/2} \left(W dy - \sigma_{xx} \frac{\partial u_x}{\partial x}\, dy \right)$$

Noting that $e_{xx} = \partial u_x / \partial x$, we have

$$\sigma_{xx} \frac{\partial u_x}{\partial x} = 2W$$

and

$$J = -\int_{h/2}^{-h/2} W dy = \int_{-h/2}^{h/2} W dy$$

Because of symmetry

$$J = 2 \int_0^{h/2} W dy$$

Shifting the origin of the y-axis to the neutral axis of the upper leg, that is, $y' = y - h/4$, the preceding integral becomes

$$J = 2\int_{-h/4}^{h/4} W dy'$$

For the upper leg,

$$\sigma_{xx} = \frac{M_0 y'}{I}, \qquad I = \frac{(h/2)^3}{12} = \frac{h^3}{96}$$

and

$$W = \frac{1}{2}\,\sigma_{xx} e_{xx} = \frac{\sigma_{xx}^2}{2E} = \frac{M_0^2 y'^2}{2EI^2}$$

We finally obtain

$$J = \frac{M_0^2}{EI}$$

which can easily be shown to be the strain energy release rate by using the compliance method.

4.4 STRESS INTENSITY FACTOR CALCULATIONS USING THE FINITE ELEMENT METHOD

The finite element method is commonly used in the stress analyses of complex engineering structures. Various techniques have been introduced to calculate stress intensity factors and energy release rates. Two commonly used methods are briefly described next.

4.4.1 Direct Method

The direct method utilizes the near-tip stress and displacement fields along the x-axis and their relations with stress intensity factors, that is,

$$\sigma_{yy} = \frac{K_I}{\sqrt{2\pi x}}, \quad x \to 0^+$$

$$u_y = \frac{K_I(\kappa + 1)}{4\mu\pi}\sqrt{-2\pi x}, \quad x \to 0^-$$

Thus,

$$K_I = \sigma_{yy}\sqrt{2\pi x}, \quad x \to 0^+$$

$$K_I = \frac{2\mu u_y}{\kappa + 1}\sqrt{\frac{2\pi}{-x}}, \quad x \to 0^-$$

where the origin of the x-axis resides at the crack tip. By plotting $\sigma_{yy}\sqrt{2\pi x}$ ($u_y\sqrt{-2\pi/x}$) versus x ($-x$) using the data of σ_{yy} (u_y) obtained from the finite element solution, the previous expressions indicate that the stress intensity factor K_I can be obtained within some distances from the crack tip where the plot approximately follows a horizontal straight line. In general, the value obtained from the displacement solution is more accurate.

This technique usually requires very fine element meshes in the vicinity of the crack tip in order to obtain a more accurate singular stress field. This may yield a large number of degrees of freedom and, thus, lead to more computing time. An alternative is to use special singular finite elements to surround the crack tip. Common to these singular finite elements is that they contain the proper $r^{-1/2}$ stress singularity terms in the displacement functions, which allow one to use relatively coarse meshes in the crack tip region.

4.4.2 Modified Crack Closure Technique

A popular and efficient method is to use regular finite elements to simulate the crack closure integral presented in Section 4.2. This procedure involves solving two problems, one before crack extension and the second after a virtual crack extension (see Figure 4.7). The energy released during crack extension is equal to the work done in closing the opened surfaces.

For the purpose of illustration, consider the finite element mesh near the crack tip as shown in Figure 4.7. Let the nodal forces at node $c(d)$ before crack extension be denoted by $F_x^{(c)}$ and $F_y^{(c)}$ for the horizontal and vertical components, respectively.

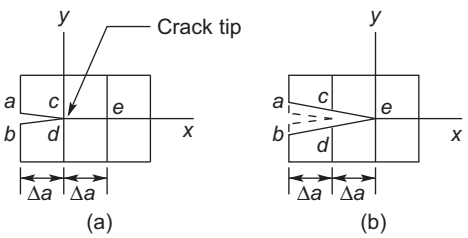

FIGURE 4.7

Virtual crack extension simulated by finite elements.

After crack extension, nodes c and d separate and their displacements are given by

$$u_x^{(c)} = \text{horizontal displacement at node } c$$
$$u_y^{(c)} = \text{vertical displacement at node } c$$
$$u_x^{(d)} = \text{horizontal displacement at node } d$$
$$u_y^{(d)} = \text{vertical displacement at node } d$$

The work done in the crack closure process can be divided into Mode I and Mode II corresponding to the opening and sliding displacements, respectively. We thus have

$$G_I = \frac{1}{2\Delta a} F_y^{(c)} \left(u_y^{(c)} - u_y^{(d)} \right)$$
$$G_{II} = \frac{1}{2\Delta a} F_x^{(c)} \left(u_x^{(c)} - u_x^{(d)} \right)$$

In this method, the virtual crack extension Δa should be small. From experience, $\Delta a/a \leq 0.05$ should be adequate.

Since $\Delta a/a$ is usually very small, the nodal displacements at nodes c and d after virtual crack extension can be approximated by the nodal displacements at nodes a and b, respectively, before virtual crack extension, that is,

$$G_I = \frac{1}{2\Delta a} F_y^{(c)} \left(u_y^{(a)} - u_y^{(b)} \right)$$
$$G_{II} = \frac{1}{2\Delta a} F_x^{(c)} \left(u_x^{(a)} - u_x^{(b)} \right)$$

Thus, there is no need to solve two problems. This is the so-called modified crack closure (MCC) method (Rybicki and Kanninen [4-8]). It should be noted that, in using the MCC method, the finite element mesh near the crack tip must be uniform. Once the energy release rates G_I and G_{II} are known, the stress intensity factors K_I and K_{II} can be calculated from Eqs. (4.10) and (4.13), respectively.

4.5 THREE-DIMENSIONAL FIELD NEAR CRACK FRONT

Most LEFM problems have been simplified and modeled as two-dimensional (2-D), though three-dimensional (3-D) effects are often acknowledged. 2-D plane strain and plane stress states are often assumed to approximate thin and thick bodies, respectively. Moreover, the plane stress formulation is not exact elasticity formulation since it does not satisfy all compatibility conditions. The error resulting from this can be significant where stress gradients are large. In view of the stress singularity at the crack tip in linearly elastic solids, the solutions of 2-D crack problems need to be reexamined from the 3-D point of view. Closed-form solutions, however,

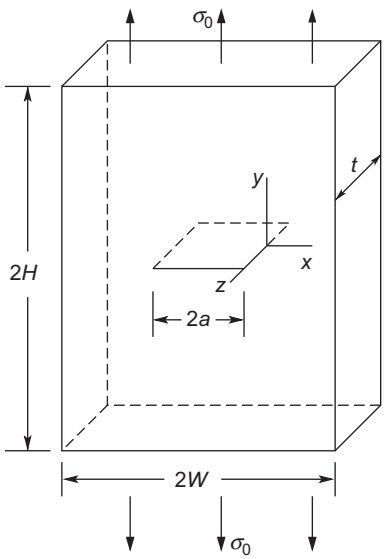

FIGURE 4.8

A through-thickness crack in an elastic plate subjected to uniform tensile stress σ_0.

are generally not available for 3-D crack problems, and finite elements and other numerical methods are usually used.

Consider a flat plate containing a center crack subjected to uniform tension as shown in Figure 4.8. Numerical solutions of the problem have been obtained in [4-9]–[4-13]. This section introduces the numerical results of Kwon and Sun [4-13] in which the dimensions of the cracked plate were taken as $W = 2a$, $H = 4a$, and $a = 12.7\ cm$. The MCC technique was used to compute energy release rate and stress intensity factors.

4.5.1 Distribution of Stress Intensity Factor over Thickness

Figure 4.9 shows the opening stress σ_{yy} (normalized by $K_0/\sqrt{2\pi x}$ where $K_0 = \sigma_0\sqrt{\pi a}$) near the crack front at different locations in the thickness direction. It is evident that, near the mid-plane of the plate ($z/t \to 0$), $\sigma_{yy}\sqrt{2\pi x}$ appears to be a constant implying that the normal stress has inverse square root singularity. However, the curves of $\sigma_{yy}\sqrt{2\pi x}$ near the plate free surface ($z/t \to 0.5$) are seen to drop and then go upward as they approach the crack front. This upswing trend is more severe near the plate free surface. This is why many researchers could not obtain the nearly zero stress intensity factor at the free surface even though very fine meshes were used in the finite element analysis.

It was shown by Su and Sun [4-14] that the stress intensity factor must drop to zero at the plate surface, but this is difficult to obtain by the finite element analysis. If more

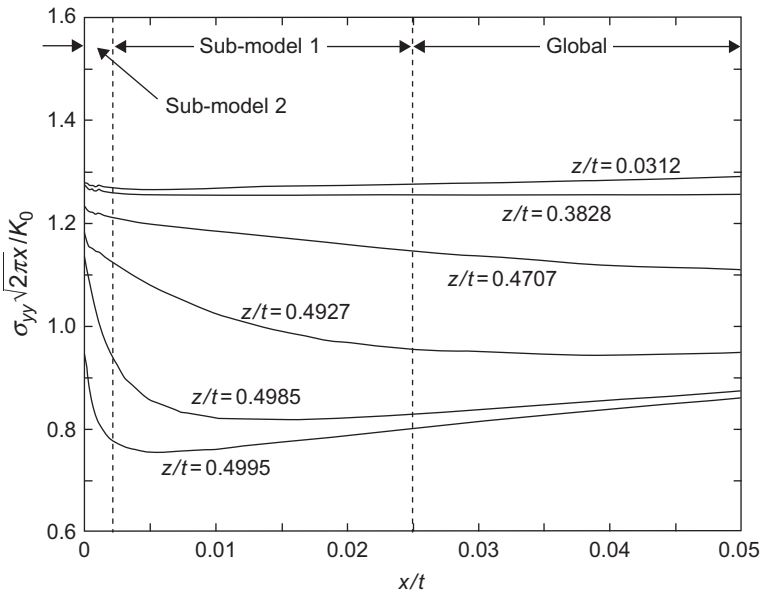

FIGURE 4.9

Normalized stress versus x/t at different z locations (adapted from Kwon and Sun [4-13]).

refined meshes in the z-direction are used, this upswing characteristic would become even more pronounced since there is another so-called (weaker) vertex singularity, which exists at the intersection between the crack front and the plate surface [4-15].

For small values of θ, Benthem [4-15] showed that the crack tip opening stress in the crack plane is expressed in the form

$$\sigma_{yy} = \frac{V}{\sqrt{2\pi\theta}}\rho^{-\lambda}$$

where ρ is the distance from the corner point, θ is the angle measured from the z-axis to the ρ direction in the $x-z$ plane, and V is the vertex stress intensity factor. For Poisson's ratio $\nu = 0.3$, the value of λ is around 0.45. Thus, besides the inverse square root stress singularity along the crack front, there is another stress singularity of lesser degree at the intersection point of the crack front and the plate surface (or the corner point).

Figure 4.10 shows the 3-D strain energy release rate obtained by the 3-D MCC method. 2-D plane stress and plane strain energy release rates that are obtained by the MCC are also plotted. All strain energy release rates are nondimensionalized by the 2-D plane strain energy release rate G_0:

$$G_0 = \frac{1-\nu^2}{E}K_0^2 = \frac{1-\nu^2}{E}\sigma_0^2(\pi a)$$

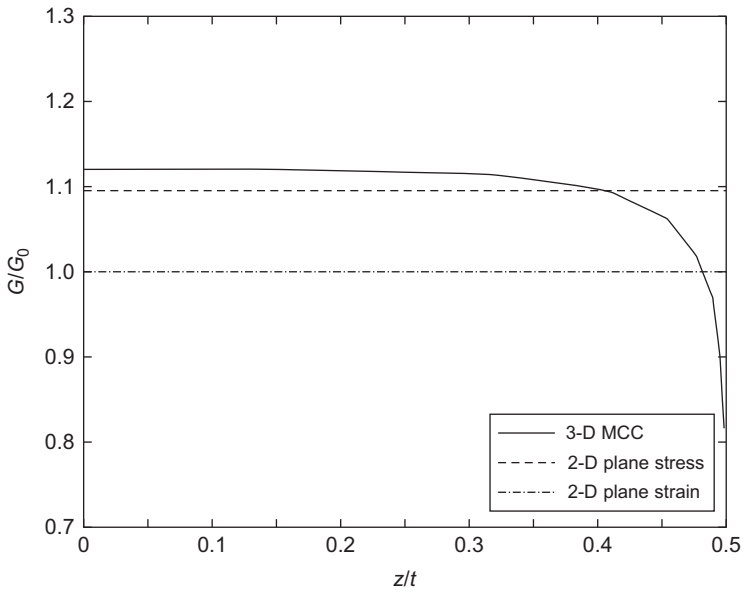

FIGURE 4.10

3-D energy release rate along the crack front and the 2-D counterparts (adapted from Kwon and Sun [4-13]).

It is shown that the strain energy release rate of the 3-D solution is closer to that of the 2-D plane stress than 2-D plane strain even though the state of the crack front is in a state of plane strain.

The stress intensity factor was obtained from the energy release rate with the plane strain conversion relation,

$$G = \frac{(1-\nu^2)K^2}{E} \tag{4.36}$$

because the state of deformation is mostly plane strain along the crack front. Figure 4.11 shows the distribution of K over the plate thickness obtained using the 3-D energy release rate for the case $t = a$ in conjunction with the $G - K$ relation. The result obtained with the stress method is also presented in the figure. It is noted that the 3-D stress intensity factor K_{3D} at the mid-plane is larger than the 2-D stress intensity factor K_{2D}. Figure 4.12 presents the distribution of these stress intensity factors for various plate thicknesses. It is noted that, except for plates with very large thicknesses, the value of K_{2D} is quite different from that of K_{3D} at the mid-plane.

A simple technique without 3-D calculations was proposed by Kwon and Sun [4-13] for evaluating approximate values of K_{3D} at the mid-plane of the plate. The 3-D energy release rate is approximated by the 2-D plane stress (rather than plane strain) counterpart for $t \leq a$. Then this energy release rate is converted to the stress

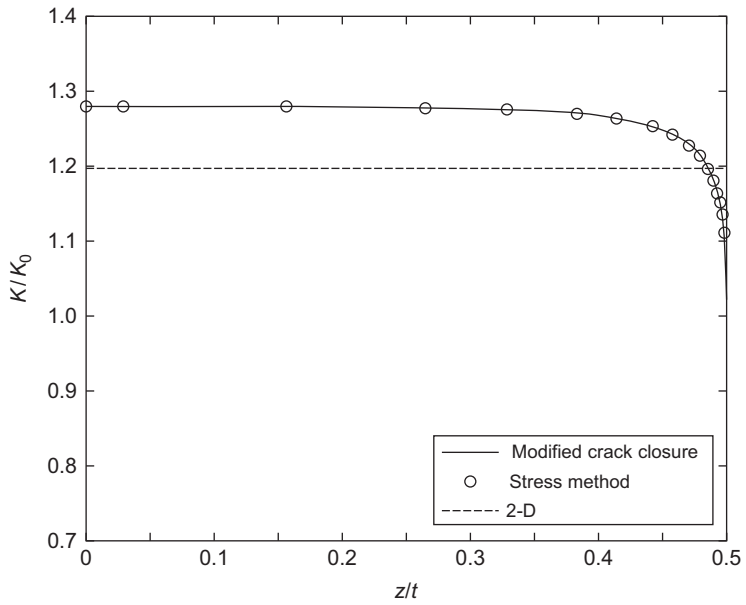

FIGURE 4.11

3-D stress intensity factor along the crack front and the 2-D counterpart (adapted from Kwon and Sun [4-13]).

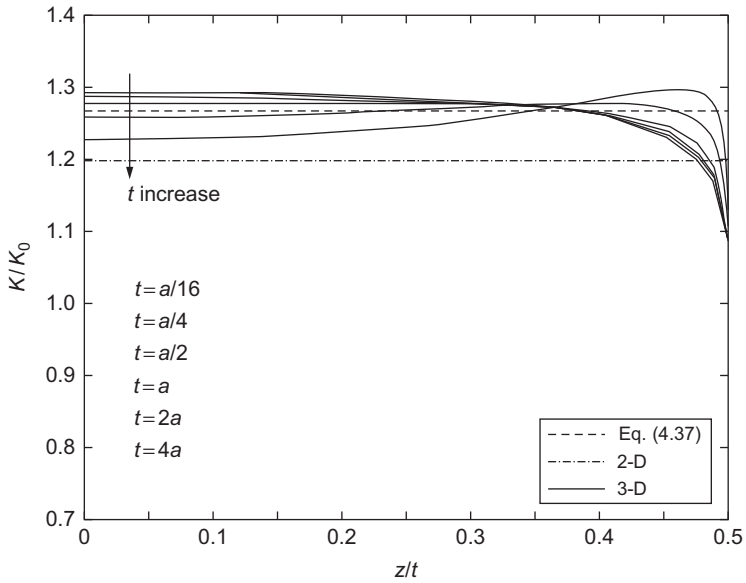

FIGURE 4.12

Stress intensity factor along the crack front for various plate thicknesses (adapted from Kwon and Sun [4-13]).

intensity factor by the plane strain $G-K$ conversion relation Eq. (4.36). With this procedure the relation between K_{3D} and K_{2D} at the mid-plane can be expressed in the form

$$\frac{K_{3D}}{K_{2D}} = \sqrt{\frac{1}{1-\nu^2}} \tag{4.37}$$

Figure 4.12 shows the prediction of K_{3D} from K_{2D} using relation Eq. (4.37). It is evident that this method is accurate except for locations near the plate surface. Relation Eq. (4.37) could be applied not only to the center-cracked plate but also to other types of specimens such as the compact tension, three point bending, and single-edge crack specimens when $t \leq a$ [4-16].

4.5.2 Plane Strain Zone at the Crack Front

The stress field near the crack front is 3-D. However, the deformation field very close to the crack front approaches a state of plane strain, while away from the crack front it approaches a state of plane stress. Between these two states, the deformation is 3-D. The 3-D region in the cracked plate is often characterized using the parameter called

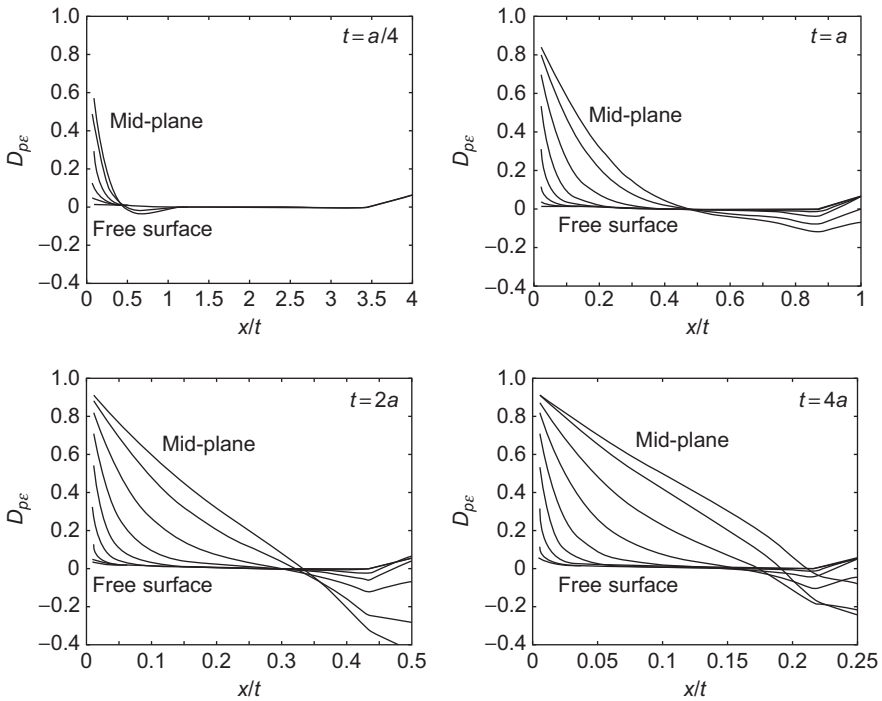

FIGURE 4.13

Degree of plane strain near the crack front for various plate thicknesses (adapted from Kwon and Sun [4-13]).

"degree of plane strain," which is defined as

$$D_{p\epsilon} = \frac{\sigma_{zz}}{\nu(\sigma_{xx} + \sigma_{yy})}$$

The parameter $D_{p\epsilon}$ is zero where the stress state is plane stress, and is unity where the stress state is plane strain. The size of the plane strain zone depends on the plate thickness.

The degrees of plane strain for different plate thicknesses are shown in Figure 4.13. In the figure, the degree of plane strain curves at different locations in the thickness direction are plotted along the crack plane. It is evident that the plane strain zone near the mid-plane of the plate is much greater than that near the plate surface. The result indicates that, for $t \leq a$, the plane strain zone size near the mid-plane of the plate is about half the plate thickness. Thus, as plate thickness decreases, the absolute size of the plane strain zone also decreases and approaches zero as $t \to 0$.

The result in Figure 4.12 clearly indicates that the stress intensity factor at the mid-plane approaches K_{2D} as the plate thickness increases beyond, say, $t = 4a$. In other words, the 2-D plane strain near-tip solution is a good approximation of the field for only very thick plates.

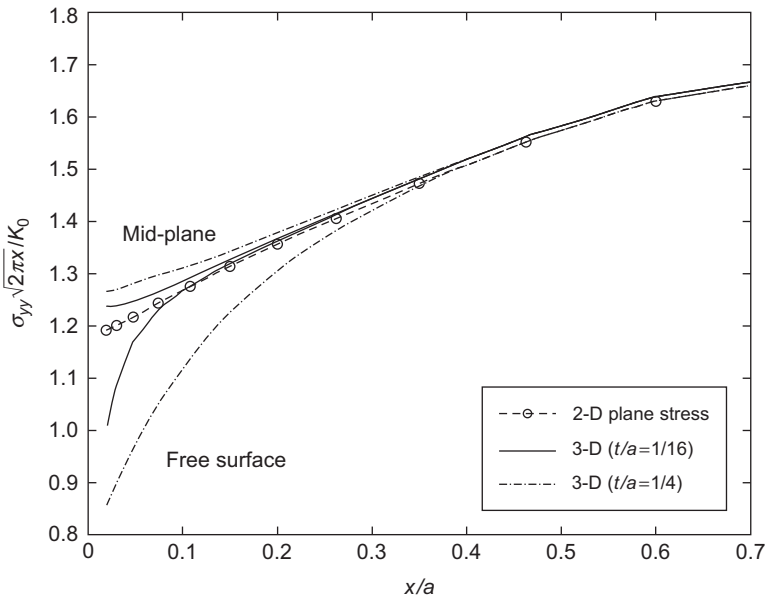

FIGURE 4.14

3-D stress field near the crack front and the 2-D plane stress counterpart (adapted from Kwon and Sun [4-13]).

On the other hand, it is shown in Figure 4.14 that 3-D stresses coincide with the plane stress solution beyond the 3-D region and that the absolute size of the 3-D region decreases as plate thickness decreases. For plates with $t \to 0$, the 3-D stress region becomes vanishingly small, and the stress intensity in the near-tip neighborhood effectively assumes the value of K_{2D}. In fact, if the 3-D region shrinks to the extent that it becomes much smaller than the fracture process zone, then the 2-D plane stress field rather than the 3-D singular field would control the fracture process.

References

[4-1] G.R. Irwin, Analysis of stresses and strains near the end of a crack traversing a plate, J. Appl. Mech. 24 (1957) 361–364.

[4-2] G.R. Irwin, Fractre dynamics, in: Fracture of Metals, American Society of Metals, Cleveland, OH, 1948, pp. 147–66.

[4-3] E. Orowan, Fundamentals of brittle fracture behavior of metals, in: Fracture and Strength of Solids, Rep. Prog. Phys. 12 (1949) 185–232.

[4-4] J.R. Rice, Mathematical analysis in the mechanics of fracture, in: H. Liebowitz (Ed.), Fracture, vol. 2, Academic Press, New York, 1968, pp. 191–311.

[4-5] J.R. Rice, A path independent integral and the approximate analysis of strain concentration by notches and cracks, J. Appl. Mech. 35 (1968) 379–386.

[4-6] Z.-H. Jin, C.T. Sun, On *J*-integral and potential energy variation, Int. J. Fract. 126 (2004) L19–L24.

[4-7] G.P. Cherepanov, Mechanics of Brittle Fracture, McGraw-Hill, New York, 1979, p. 240.

[4-8] E.F. Rybicki, M.F. Kanninen, A finite element calculation of stress intensity factors by a modified crack closure integral, Eng. Fract. Mech. 9 (1977) 931–938.

[4-9] D.J. Ayres, A numerical procedure for calculating stress and deformation near a slit in a three-dimensional elastic-plastic solid, Eng. Fract. Mech. 2 (1970) 87–106.

[4-10] T.A. Cruse, Three-dimensional elastic stress analysis of a fracture specimen with an edge crack, Int. J. Fract. Mech. 7 (1971) 1–15.

[4-11] T. Nakamura, D.M. Parks, Three-dimensional stress field near the crack front of a thin elastic plate, J. Appl. Mech. 55 (1988) 805–813.

[4-12] K.N. Shivakumar, I.S. Raju, Treatment of singularities in cracked bodies, Int. J. Fract. 45 (1990) 159–178.

[4-13] S.W. Kwon, C.T. Sun, Characteristics of three-dimensional stress fields in plates with a through-the-thickness crack, Int. J. Fract. 104 (2000) 291–315.

[4-14] X.M. Su, C.T. Sun, On singular stress at the crack tip of a thick plate under in-plane loading, Int. J. Fract. 82 (1996) 237–252.

[4-15] J.P. Benthem, State of stress at the vertex of a quarter-infinite crack in a half-space, Int. J. Solids Struct. 13 (1977) 479–492.

[4-16] G. Yagawa, T. Nishioka, Three-dimensional finite element analysis for through-wall crack in thick plate, Int. J. Numer. Methods Eng. 12 (1978) 1295–1310.

PROBLEMS

4.1 Use the J-integral and the compliance method to calculate the strain energy release rate for the double cantilever beam shown in Figure 4.15. Assume the thickness of the beam to be unity.

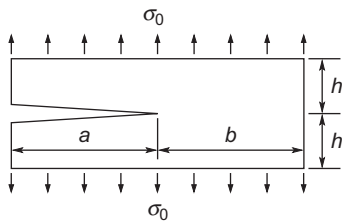

FIGURE 4.15

A double cantilever beam under uniform transverse loading.

4.2 Use plane strain or plane stress 2-D finite elements to model the split beam of Figure 4.15. Calculate the strain energy release rate using the crack closure method and compare with the results obtained in Problem 4.1. Also use the near-tip stresses obtained from the finite element analysis to extract the stress intensity factor. Compare with the results obtained in Problem 4.1 using other methods. Assume $a=b=10$ cm, $h=1$ cm, $\sigma_0=2$ MPa, $E=70$ GPa, $\nu=0.25$.

4.3 Find G_I and G_{II} of the split beam (of unit width) loaded as shown in Figure 4.16 by using the compliance method described in Chapter 2 and by the J-integral.

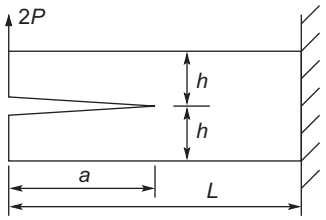

FIGURE 4.16

A split beam under a concentrated load.

4.4 Use the Mode I near-tip solutions for the stress and displacement fields to calculate the J-integral, and show that $G_I = K_I/E$ for plane stress problems.

4.5 Use plane stress finite elements to model the problem given in Figure 4.16, and calculate G_I and G_{II} using the MCC method and the compliance method. Consider the following two cases:

1. $a = 5$ cm, $h = 2$ cm, $L = 20$ cm, $P = 2$ kN
2. $a = 12$ cm, $h = 2$ cm, $L = 20$ cm, $P = 2$ kN

Compare the finite elements results with those obtained in Problem 4.4.

4.6 Use plane strain or plane stress 2-D finites elements to model the edge-cracked plate loaded as shown in Figure 4.17. Extract the stress intensity factor and compare the results using the following.

1. Stresses ahead of the crack tip (plot $\sqrt{2\pi x}\sigma_{yy}$ vs x curve near the crack tip).
2. Displacements of the crack surface (plot $\frac{4\mu u_y}{\kappa+1}\sqrt{\frac{\pi}{2r}}$ vs x curve near the crack tip).
3. Crack closure method.

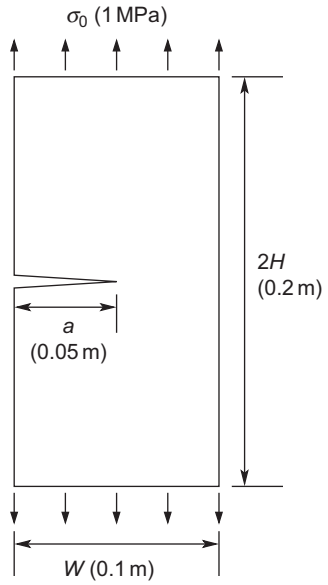

FIGURE 4.17
An edge cracked plate subjected to tension.